The Astrophysical Journal Letters, 733:L41 (4pp), 2011 June 1 doi:10.1088/2041-8205/733/2/L41

PLANETESIMAL FORMATION INDUCED BY SINTERING

Sin-iti Sirono
Earth and Environmental Sciences, Nagoya University, Tikusa-ku, Furo-cho, Nagoya 464-8601, Japan
Received 2011 March 4; accepted 2011 April 25; published 2011 May 11

ABSTRACT

Sintering of H_2O ice proceeds in an icy dust aggregate as the temperature increases due to the infall to the central star. By numerical simulations, I show that fragmentation of the aggregate by sintering occurs at a particular region of a protoplanetary nebula. The fragments accumulate at the region because their infalling velocity is low. The dust surface density exceeds the critical surface density required for gravitational instability to form planetesimals.

Key words: planets and satellites: formation – protoplanetary disks

Online-only material: animation, color figures

1. INTRODUCTION

A planetesimal is an object that is 1–10 km in size from which the planets in our solar system are believed to have originated. However, theories regarding its formation process remain controversial. Gravitational instability (Goldreich & Ward 1973) of a dust-rich sublayer is a convincing model that can be used to explain its formation; however, it requires a dust-to-gas surface density ratio that is 5–20 times (Sekiya 1998) greater than normal cosmic values. Many models have been proposed to enhance this ratio such that the gravitational instability is triggered; they include model based on dust concentration by turbulence eddies (Cuzzi et al. 2001), streaming instability (Johansen et al. 2007), radial drift of aggregates (Youdin & Shu 2002), anti-cyclonic vortices (Chavanis 2000), photoevaporation by UV rays (Throop & Bally 2005), gas pressure maxima associated with the snow line (Brauer et al. 2008b), and the change in the activity of magnetorotational instability at the snow line (Kretke & Lin 2007).

Submicron-sized dust grains in a protoplanetary nebula collide with one another and form aggregates in which the dust grains are connected by surface adhesion. In low-temperature region, the main component of the grain is H_2O ice (Sunshine et al. 2007). The infall of the aggregates to the central star occurs because of gas drag, and the temperature of the aggregate rises. H_2O molecules move to the neck between adjacent grains when the temperature rises. This process is called as sintering (for a detailed review, see Moya et al. 2002). There are several molecular transport mechanisms involved in sintering, such as surface diffusion, grain boundary diffusion, lattice diffusion, plastic flow, and vapor transport. For H_2O ice (Blackford 2007), the convincing dominant mechanism is vapor transport at low temperatures in a protoplanetary nebula environment.

In this Letter, I show how capillary instability (Nichols & Mullins 1965), followed by the sintering of H_2O ice, effectively increases this ratio locally. Fragments from dust aggregates stagnate around the heliocentric distance where sintering occurs. Saito & Sirono (2011) proposed a mechanism of the formation of a rocky planetesimal by sublimation of icy components in contrast to this study, where icy planetesimal formation is investigated.

2. SINTERING FRAGMENTATION

It is highly probable that the packing fraction of the aggregate is quite small and that the basic structure of the aggregate is a chain of grains (Blum et al. 2000). Sintering leads to the formation of cylinders from the chain of grains (for SiO_2 particles, see Poppe 2003). It is widely known that a liquid cylinder is unstable because of its capillarity; this phenomenon was discovered by Lord Rayleigh (1892). Likewise, a solid cylinder is unstable because of capillarity. For example, it has been analytically shown that a solid cylinder is unstable if surface diffusion proceeds on the cylinder (Nichols & Mullins 1965). Surface diffusion on a fractal aggregate of silver grains results in fragmentation of the aggregate (Brèchignac et al. 2002). A snowflake kept at a temperature that is slightly higher than its melting temperature fragments into small pieces because of the viscous flow of liquid H_2O (Fujiyoshi & Muramoto 1996).

Vapor transport is driven by the surface curvature. The equilibrium vapor pressure on a curved surface differs from that on a flat surface. The difference in the pressure is proportional to the surface curvature $K (= 1/R_1 + 1/R_2$, where R_1 and R_2 are the principal radii of curvature). A bumped surface has a positive K, and a dipped one has a negative K. The H_2O molecules on a large positive K surface sublimate and condense on a surface with negative K. The rate of growth (or shrinkage) of a surface dr/dt is given by (Flin et al. 2003)

$$\frac{dr}{dt} = \frac{P_e(T)\gamma\Omega^2}{\sqrt{2\pi m_{H_2O} k_B^3 T^3}}(\bar{K} - K), \quad (1)$$

where $P_e(T)$ is the equilibrium vapor pressure of H_2O on a flat surface; γ, the surface energy of H_2O ice; Ω, the molecular volume of H_2O; m_{H_2O}, the molecular mass of H_2O; k_B, the Boltzmann constant; and $\bar{K}$, the average curvature. The last term is based on the assumption that the sublimation and condensation equilibrium is attained; the amounts of molecules undergoing sublimation and condensation are equal (this equilibrium is quickly in a typical solar nebula environment). It should be noted that the equation is applicable when the mean free path of the vapor is less than the grain size. However, Equation (1) is a very good approximation even when the mean free path is larger than the grain size (Sirono 2011). From the above equation, we see that the timescale τ_a required for the shrinkage of a grain with radius a is $\tau_a = a^2\sqrt{2\pi m_{H_2O} k_B^3 T^3}/P_e(T)\gamma\Omega^2$.

If the disconnection (disappearance of small particles) occurs under the Earth's gravity, a fluffy aggregate of icy particles will quickly densify because the disconnected part will fall until it finds a stable position. Experimentally, the quick densification of a snow pack is indeed observed at the initial stage of sintering

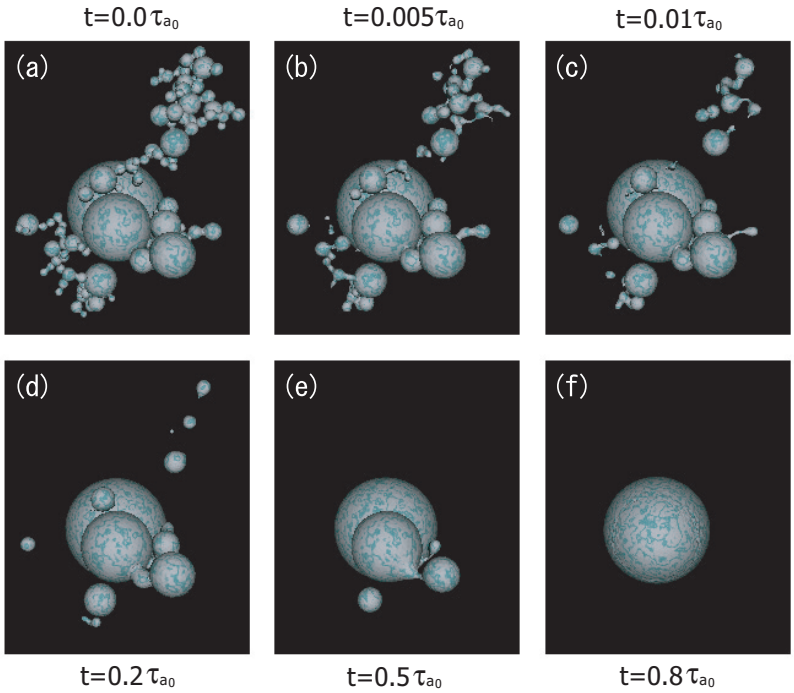

Figure 1. Snapshots of the evolution of an H_2O icy aggregate composed of 128 spherical grains. The size distribution of the grains is given by $n(a) \propto a^{-3.5}$ with the size range $0.1a_0 < a < 2a_0$, where a_0 is the typical radius of the grain. Time in the simulation is normalized by τ_{a_0} (see the text). The snapshots are taken when $t =$ 0, 0.005, 0.01, 0.02, 0.05, 0.8 in the normalized unit. The formation of cylinders is seen in panels (b) and (c). The cylinders are unstable and disconnect to fragments (c and d). If a region with a large positive curvature is formed, disconnection proceeds even in the late stage (e). Finally, only one large spherical fragment survives; all the H_2O molecules condense on this fragment (f).

(An animation and a color version of this figure are available in the online journal.)

(Flin 2004). The occurrence of standard volumetric sintering is too slow to explain the quick densification. The density evolution is well explained by the numerical simulation (Flin 2004) of vapor diffusion sintering, including the effects caused by the disconnection. Moreover, the development of X-ray tomography enables us to determine the three-dimensional internal structure of snow packs in detail, including the evolutions of the average curvature and the total surface area. Both the evolutions are well explained by simulations of vapor transport sintering (Flin et al. 2003).

The numerical simulation of sintering of the H_2O aggregate caused by vapor transport is performed to investigate the evolution of the size and the number of fragments produced from an aggregate. An aggregate is composed of spherical grains and is arranged by ballistic–cluster–cluster aggregation (BCCA) and ballistic–particle–cluster aggregation (BPCA; Meakin 1988). A BCCA aggregate is highly porous, in contrast to a BPCA aggregate which has a compact structure. The size distribution of composing grains is given by (Mathis et al. 1977) $n(a) \propto a^{-3.5}$ ($0.1a_0 \leqslant a \leqslant 2a_0$ (BCCA) and $0.25a_0 \leqslant a \leqslant 0.5a_0$ (BPCA), where a_0 is the representative radius of the grains). For simplicity, a silicate core inside an icy grain is neglected taking into account the low volume fraction ($\sim$10%) of the core. This is because the mass ratio of ices to silicates is $\simeq$4 (Hayashi et al. 1985) and the density ratio of silicates to ices is $\simeq$3.

It should be noted that Equation (1) can be rearranged in a normalized form in which the time is measured by τ_{a_0}. In order to numerically integrate Equation (1), the surface of an aggregate is covered by a triangular mesh. The surface curvature for each mesh point is determined by the method in Garimella & Swartz (2000). Then, the motion of each mesh point is obtained according to Equation (1). If the radius of a neck becomes less than $0.01a_0$, the neck is disconnected and new mesh points cover the two newly formed surfaces instead of the neck. This threshold is placed to avoid numerical instability. If the radius becomes less than $0.01a_0$, the neck radius inevitably goes to zero, which is confirmed by a separate two-dimensional simulation.

Figure 1 shows snapshots of the evolution of a BCCA aggregate composed of 128 grains. The necks between the grains grow initially because the curvature of a neck is negatively large. On the other hand, surfaces of small grains shrink because of their large positive curvatures. The combination of these two effects leads to the formation of cylinders (see Figures 1(b) and (c)). The cylinders are unstable because of their large positive curvatures that are perpendicular to the cylinders' axes. Shrinkage proceeds in a cylinder, and eventually, disconnection takes place. The size of the fragments is much smaller than the size of the original aggregate. The shapes of the fragments evolve from irregular to spherical because of vapor transport. Sublimation proceeds on small fragments and condensation on the large fragments. Finally, only one large spherical fragment survives; all the H_2O molecules condense on this fragment (Figure 1(f)). It should be noted that disconnection occurs not only in the initial stage but also in the later stage of the evolution (Figure 1(e)) depending on the shape of the evolving fragments.

Figure 2 shows the time evolution of the number of fragments. A fragment is defined as a connected component in a simulation. According to this definition, the initial and the final number of fragments are unity. At the first stage, cylinders formed by

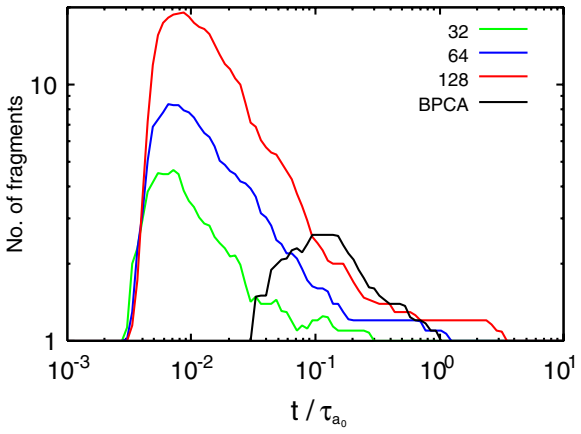

Figure 2. Time evolution of the number of fragments. The number starts from unity (the original aggregate: Figure 1(a)) and ends at unity (a totally merged sphere: Figure 1(f)). The red, blue, and green curves are the results of the BCCA aggregates with 32, 64, and 128 grains, respectively. The black curve is the result of BPCA aggregates with 32 grains. Each curve is the average of 10 different aggregates. At the first stage, cylinders formed by small grains disconnect, and the number of fragments increases. All curves for BCCA aggregates reach the peak at $t \simeq 0.01\tau_{a_0}$. For the BPCA aggregates, the peak is $t \simeq 0.1\tau_{a_0}$. The fragment number decreases after the peak because of the disappearance of small fragments due to sublimation.

(A color version of this figure is available in the online journal.)

small grains disconnect and the number of fragments increases. The peak in the fragment number occurs at $t \simeq 0.01\tau_{a_0}$ for BCCAs and at $t \simeq 0.12\tau_{a_0}$ for BPCAs, which is close to the timescale of shrinkage for the smallest grain (it should be noted that $\tau_a \propto a^2$; the timescale for a radius of $0.1a_0$ is $0.01\tau_{a_0}$, and for $0.25a_0$ is $0.063\tau_{a_0}$). Therefore, we see that the fragmentation of an aggregate is determined by small grains. The fragment number slowly decreases after the peak because the small fragments disappear because of sublimation. Through sublimation, a silicate core inside an icy grain may be released. This core sticks to the icy fragments in short timescale determined by the Brownian motion (∼0.1 yr).

3. ACCUMULATION OF FRAGMENTS

We have confirmed that an icy aggregate breaks up in the timescale of $\tau_a(T)$, where a is a typical radius of small grains. It should be noted that the temperature T depends on the heliocentric distance in a protoplanetary nebula. When $\tau_a(T)$ becomes comparable to the infalling timescale of an aggregate, the aggregate breaks up.

As the aggregates break up, the dust-to-gas surface density ratio increases locally because the infalling velocity of the fragments substantially drops from that of the original aggregate. Figure 3 displays the evolution of dust surface density. This is a result of a numerical simulation essentially same as that previously carried out (Brauer et al. 2008a). The radial coordinate of a protoplanetary disk is divided into bins in which the coagulation equation is solved to determine the size distribution of aggregates. Aggregates drift inward by gas drag in addition to the inward gas accretion onto the central star, and diffuse inward and outward by turbulent diffusion. All quantities are vertically integrated as done by Brauer et al. (2008a). The initial dust surface density is that for the minimum mass solar nebular model (Hayashi et al. 1985). The turbulence parameter is $\alpha = 10^{-3}$ which leads to the diffusion of fragments. The radius of a monomer is $0.5\,\mu$m. The temperature distribution (Kennedy & Kenyon 2008) is adopted with an accretion rate of

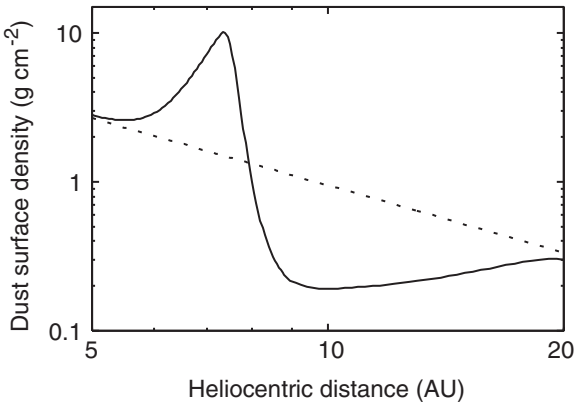

Figure 3. Evolution of the dust surface density distribution. The dotted line is the initial distribution (Hayashi et al. 1985). The solid line is the distribution after 9×10^3 yr. At 7.4 AU, a peak is formed and the surface density is enhanced more than a factor of six, which is a criterion for gravitational instability (Sekiya 1998).

$\dot{M} = 10^{-7}\,M_\odot\,\mathrm{yr}^{-1}$. The snow line in this model is located at 6.6 AU. Perfect sticking of aggregates is assumed, and impact fragmentation is not included. Packing fraction of the aggregates is assumed to be 0.01. The simulated area is between 7 and 40 AU. The sintering fragmentation is included by reducing the number of aggregates n as $dn/dt \propto \exp(-t/\tau_a(T))$, and increasing the number of monomers (unit grains) such that the total mass is kept constant. In the sintering timescale $\tau_a(T)$, $a = 0.5\,\mu$m is adopted.

In 9×10^3 yr, the dust surface density at 7.4 AU is enhanced by a factor of 6.7, which is larger than a criterion for gravitational instability (Sekiya 1998).

Coagulation cannot proceed within 7.4 AU because the timescale of fragmentation is too short. After fragmentation, small part of fragments may grow by condensation. The timescale for growth to a size a at 7.4 AU ($T = 127$ K) is given by $\tau_a = 1250(a/0.5\,\mu\mathrm{m})^2$ yr. Therefore, some fragments may grow up to micron size (this effect is not included in the simulation). However, the infall velocity of the fragments is still negligible. Even if we wait 10^6 yr, the radius a becomes only $14\,\mu$m. If the monomer size in the simulation is increased by a factor of 10, the sintering timescale increases by a factor of 100. The temperature increase to compensate this increase in the timescale by a factor of 100 is 14 K. This corresponds to a inner shift of the fragmentation region by 0.3 AU. Likewise, if the monomer size is decreased by a factor of 10, the fragmentation region shifts outward by 0.2 AU.

If the fragments reaccumulate on the infalling aggregates, the enhancement is delayed. However, the rotation of an aggregate will prevent the fragment from reaccumulating on the original aggregate from which it split off. Consider that the aggregate rotates with an angular velocity Ω. The fragmentation proceeds from the surface of the aggregate to the interior with the conduction of heat. The fragment from the surface of the aggregate has a velocity ΩR. The fragment travels a distance $\simeq R$ within a rotational period $1/\Omega$ of the aggregate. Such a fragment avoids a collision with irregular surfaces of the aggregate. This is possible if the stopping time of the fragment is long enough such that $\tau_{\mathrm{stop}} > 1/\Omega$. For a 0.1 m sized aggregate, this condition is violated only if the rotation of the aggregate is slow, i.e., $1/\Omega < 125$ s (for a spherical fragment of $0.5\,\mu$m radius). Moreover, even if the fragment sticks to the surface of the aggregate, the aggregate becomes unstable and

the fragment accompanying the one that sticks splits off. This process also prohibits the mutual sticking of the fragments in the accumulation region.

It should be noted that turbulence diffusion and inward migration by gas accretion are included in the model. Therefore, Figure 3 displays that the effects of diffusion and accretion are negligible on the radial accumulation of the fragments. However, the vertical settling of fragments would be prevented by the turbulence. When the turbulence stops, fragments settle to the midplane and gravitational instability become possible. Aggregates inside 20 AU infall and stagnate at the peak because of the sintering fragmentation. Succeeding infall of the aggregates produces planetesimals continuously in regions outwardly separated from the snow line.

The author greatly thanks to the critical comments by the anonymous reviewer.

REFERENCES

Blackford, J. R. 2007, J. Phys. D: Appl. Phys., 40, R355
Blum, J., et al. 2000, Phys. Rev. Lett., 85, 2426
Brauer, F., Dullemond, C. P., & Henning, Th. 2008a, A&A, 480, 859
Brauer, F., Henning, Th., & Dullemond, C. P. 2008b, A&A, 487, L1
Brèchignac, C., Cahuzac, Ph., Carlier, F., Colliex, C., Leroux, J., Masson, A., Yoon, B., & Landman, U. 2002, Phys. Rev. Lett., 88, 196103
Chavanis, P. H. 2000, ApJ, 356, 1089
Cuzzi, J. N., Hogan, R. C., Paque, J. M., & Dobrovoslskis, A. R. 2001, ApJ, 546, 496
Flin, F. 2004, PhD thesis, Univ. Grenoble 1
Flin, F., Brzoska, J.-B., Lesaffre, B., Coléou, C., & Pieritz, A. 2003, J. Phys. D: Appl. Phys., 36, A49
Fujiyoshi, Y., & Muramoto, K. 1966, J. Meteor. Soc. Japan, 74, 343
Garimella, R. V., & Swartz, B. K. 2000, Technical Report Los Alamos National Laboratory, LA-UR-03-8240
Goldreich, P., & Ward, W. R. 1973, ApJ, 183, 1051
Hayashi, C., Nakazawa, K., & Nakagawa, Y. 1985, in Protostars and Planets II, ed. D. C. Black & M. S. Matthews (Tucson, AZ: Univ. Arizona Press), 1100
Johansen, A., Oishi, J. S., Mac Low, M.-M., Klahr, H., Henning, Th., & Youdin, A. M. 2007, Nature, 448, 1022
Kennedy, G. M., & Kenyon, S. J. 2008, ApJ, 673, 502
Kretke, K. A., & Lin, D. N. C. 2007, ApJ, 644, L55
Mathis, J. S., Rumpl, W., & Nordsieck, K. H. 1977, ApJ, 217, 425
Meakin, P. 1988, Annu. Rev. Phys. Chem., 39, 237
Moya, J., Baudin, C., & Miranzo, P. 2002, in Encyclopedia of Physical Sciences and Technology, Vol. 14, ed. R. A. Meyers (3rd ed.; San Diego, CA: Academic Press), 865
Nichols, F. A., & Mullins, W. W. 1965, Trans. Metall. Soc. AIME, 233, 1840
Poppe, T. 2003, Icarus, 164, 139
Rayleigh, L. 1892, Phil. Mag., 34, 145
Saito, E., & Sirono, S. 2011, ApJ, 728, 20
Sekiya, M. 1998, Icarus, 133, 298
Sirono, S. 2011, ApJ, in press
Sunshine, J. M., Groussin, O., Schultz, P. H., A'Hearn, M. F., Feaga, L. M., Farnham, T. L., & Klassen, K. P. 2007, Icarus, 190, 284
Throop, H. B., & Bally, J. 2005, A&A, 623, L149
Youdin, A. M., & Shu, F. H. 2002, ApJ, 580, 494